Geochemistry Geophysics Geosystems G3
AN ELECTRONIC JOURNAL OF THE EARTH SCIENCES
Published by AGU and the Geochemical Society

Article
Volume 9, Number 8
20 August 2008
Q08S09, doi:10.1029/2008GC001991
ISSN: 1525-2027

Crustal structure along the southern Central American volcanic front

Laura MacKenzie
Department of Earth Sciences, Boston University, Boston, Massachusetts 02215, USA (lauger_98@yahoo.com)

Geoffrey A. Abers
Department of Earth Sciences, Boston University, Boston, Massachusetts 02215, USA

Now at Lamont-Doherty Earth Observatory, Columbia University, Palisades, New York 10964, USA

Karen M. Fischer
Department of Geological Sciences, Brown University, Providence, Rhode Island 02912, USA

Ellen M. Syracuse
Department of Earth Sciences, Boston University, Boston, Massachusetts 02215, USA

J. Marino Protti and Victor Gonzalez
Observatorio Vulcanologic y Sismologico de Costa Rica, Universidad Nacional, Apartado 2346-3000, Heredia, Costa Rica

Wilfried Strauch
Volcanology Department, Instituto Nicaraguense de Estudios Territoriales, Apartado 2110, Managua, Nicaragua

[1] Subduction alters continents several ways, including accretion, magmatic addition, mantle wedge serpentinization, and crustal differentiation. These changes affect seismic velocities, so characterizing upper plate crust establishes a baseline for composition and continental growth. Teleseismic *P* and *PP* arrivals from a temporary deployment of broadband seismometers in Central America have been used to estimate crustal thickness and *Vp/Vs* ratio from receiver functions and to image crust across the active arc. Crustal thickness ranges from 25 to 44 km with formal errors of 1.6–9.2 km. The thinnest crust (24.6 ± 3.5 km) lies directly beneath the Nicaraguan arc, whereas the thickest crust lies in the Nicaraguan back arc (43.5 ± 2.5 km) and beneath the Costa Rican arc (37.9 ± 5.2 km). Crustal structure and *Vp/Vs* show sharp transitions at terrane boundaries. The Moho exhibits strong velocity contrasts throughout the study area of ~0.5–1.0 km/s, even beneath arc and fore arc, precluding extensive serpentinization or ponded melt below the Moho. Crust is thicker beneath the Costa Rican arc, consistent with 10–23 km^3/km/Ma crustal growth. The crust is thinner by 11–18 km beneath the large depression in central Nicaragua, with the thinnest crust beneath the arc. There, the relationship between thin crust, arc location, and deeper seismic velocities suggests that upper plate structure plays a critical role in focusing magma to the surface.

Components: 10,206 words, 14 figures, 2 tables.

Keywords: Central America; Vp/Vs; crustal thickness; plate boundaries; subduction; receiver functions.

Index Terms: 7240 Seismology: Subduction zones (1207, 1219, 1240); 8038 Structural Geology: Regional crustal structure; 8104 Tectonophysics: Continental margins: convergent; 8185 Tectonophysics: Volcanic arcs.

Received 14 February 2008; **Revised** 30 April 2008; **Accepted** 2 May 2008; **Published** 20 August 2008.

MacKenzie, L., G. A. Abers, K. M. Fischer, E. M. Syracuse, J. M. Protti, V. Gonzalez, and W. Strauch (2008), Crustal structure along the southern Central American volcanic front, *Geochem. Geophys. Geosyst.*, *9*, Q08S09, doi:10.1029/2008GC001991.

Theme: Central American Subduction System

1. Introduction

[2] The recycling of mantle material at subduction zones results in generation of new crust, a surface manifestation of which is arc volcanism. Many forces drive magmatism, whose individual contributions are difficult to separate. The thickness of the crust overlying the mantle wedge has been shown to correlate with the extent of melting [*Plank and Langmuir*, 1998], with thin crust giving a higher degree of melting, presumably because there is a longer melting column. Also crustal thickness along volcanic arcs constrains continental growth rates [*Holbrook et al.*, 1999; *Klemperer*, 1989; *Reymer and Schubert*, 1984]. While present-day arc magmatism is dominated by basaltic eruptions, processes such as delamination or foundering of the lower crust could result in a more silicic and thinner continental crust, resembling that of stable continents [*Behn and Kelemen*, 2006; *Martin*, 1986; *Rudnick*, 1995; *Suyehiro et al.*, 1996].

[3] The main goal of this study is to measure both crustal thickness and a vertically averaged *Vp/Vs* for the Central America crust. The Tomography Under Costa Rica And Nicaragua (TUCAN) project provides a new data set to determine these parameters using teleseismic converted phases. This study provides the first regional study of crustal thickness variations, and, as a byproduct, crustal structure is imaged. The results show crustal thickness variations from 25 to 44 km, with the thinnest crust directly beneath the arc in Nicaragua. The data also show boundaries between crustal terranes beneath the arc through crustal thickness and *Vp/Vs* changes.

2. Tectonic Setting

[4] The Central American volcanic arc in Costa Rica and Nicaragua results from subduction of the Cocos plate beneath the Caribbean plate. Both the overriding Caribbean plate and the subducting Cocos plate vary in both age and structure. The Cocos plate subducts beneath the Caribbean plate at a rate of 80–90 mm/a, normal to the trench in southwestern Costa Rica and with 15° obliquity in northwestern Nicaragua [*Barckhausen et al.*, 2001; *Turner et al.*, 2007]. North of the Fisher Ridge offshore Costa Rica lies the EPR-CNS boundary. North of the EPR-CNS boundary the Cocos Plate, formed at the Eastern Pacific Rise, appears relatively smooth, with an age of 24 Ma at the Middle American Trench [*Barckhausen et al.*, 2001]. South of this boundary, seamounts dominate a ''rough'' segment formed at the Cocos-Nazca spreading system, with an age of 15–23 Ma off central Costa Rica. The Cocos Ridge subducts off southern Costa Rica; this unusually thick oceanic crust formed under the influence of the Galapagos hot spot 15–19 Ma [*Barckhausen et al.*, 2001] (Figure 1).

[5] The Central American volcanic arc sits upon a complex accumulation of accreted terranes. The Chorotega and Chortis blocks constitute the majority of Costa Rica and Nicaragua, respectively [e.g., *Dengo*, 1985]. While the boundaries of these blocks are obscured by widespread sedimentary and young volcanic cover, the major boundary between the two probably lies in the vicinity of the political border between Nicaragua and Costa Rica [*Baumgartner and Denyer*, 2006; *Mann et al.*, 2007]. The Chortis block is underlain by pre-Mesozoic basement rocks of North American affinity and lies beneath most of Nicaragua northeast of the arc [*Meschede and Frisch*, 1998]. The Pacific coastal region of Nicaragua has accreted to the Chortis block [*Case et al.*, 1990], and is possibly a relict arc [*Walther et al.*, 2000]. The Chorotega block composes much of Costa Rica. Its crust formed during the Mesozoic and Cenozoic as thickened oceanic crust, possibly part of the Caribbean Large Igneous Province (CLIP) [e.g., *Ball et al.*, 1969; *Pindell and Dewey*, 1982; *Sinton et al.*, 1997]. However, basement rocks are exposed only near the Pacific coast [*Hoernle et al.*, 2002].

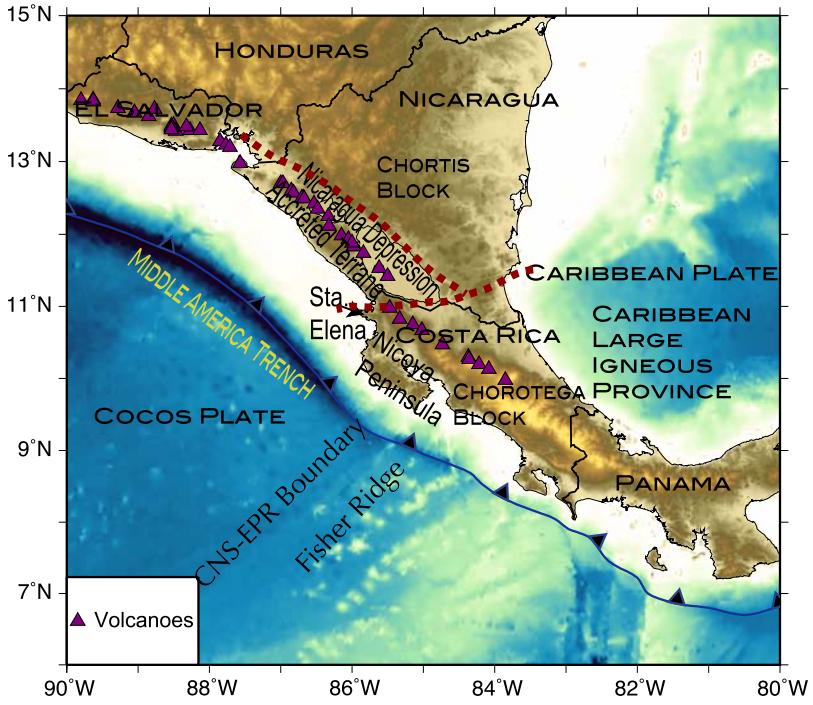

Figure 1. Map of Central America, showing major tectonic and political features. Dashed red lines indicate inferred boundaries between Chortis Block, Chorotega Block, and the Nicaragua fore-arc accreted terrane.

[6] The modern volcanic arc shows a step in distance from the trench of approximately 50 km going from Costa Rica into Nicaragua (Figure 1). The depth to slab vertically beneath the arc ranges from 150 to 180 km in Nicaragua to 80–95 km in Costa Rica across the step in the arc [*Syracuse et al.*, 2008]. It has since been shown that the slab changes smoothly in dip along this section of the arc [*Burbach et al.*, 1984; *Protti et al.*, 1994; *Syracuse and Abers*, 2006], so plate geometry does not cause the step. The arc lies on mountainous terrane in Costa Rica, but farther north it lies within the low-lying Nicaragua Depression. It migrated trenchward from the highlands over the past 25 Ma, reaching its current location between 7 and 1.5 Ma [*Ehrenborg*, 1996; *Plank et al.*, 2002; *Weinberg*, 1992]. The oldest dated lavas within the depression for the current arc are between 65 and 330 ka, with volcaniclastic cover hiding older deposits [*Carr et al.*, 2007].

[7] Previous studies have given some indication of crustal thickness in Costa Rica and Nicaragua, however a majority of the studies are offshore or are limited to a single locality. Table 1 summarizes these measurements, which vary in crustal thickness from 34 to 43 km. The only regional crustal thickness estimates are from *Carr* [1984], who assumes isostatic equilibrium to estimate crustal thickness from elevation along the volcanic front. These are not direct estimates, and may be significantly in error if dynamic forces, plate flexure, or lateral density variations contribute to elevation changes.

3. Data and Methods

[8] Crustal thickness and *Vp/Vs* are measured from receiver functions recorded across a dense broadband array in southern Central America. The receiver functions are derived from the coda of the *P* and *PP* waves following the methods of *Rondenay et al.* [2005] and *Rossi et al.* [2006]. Images produced from the receiver functions show both variations in crustal thickness and complications in crustal structure across the array.

3.1. Data Processing

[9] The TUCAN PASSCAL experiment deployed 48 broadband seismometers from July 2004 through March 2006. The stations are positioned in two along-arc transects at 50 km spacing, and two dense cross arc transects with an average spacing of 10 km (Figure 2). The seismometers are broadband sensors with 30 or 120 s free periods, which continuously recorded data at 50 samples per second. The network achieved 91% data recovery and all data are archived at the IRIS DMC. Time series from three permanent broad-

Table 1. Previous Crustal Thickness Estimates

Location	Thickness (km)	Method	Author
Arenal Volcano, northern Costa Rica	43 ± 7	travel time, passive	*Matumoto et al.* [1977]
JTS, Nicoya region	36 ± 4	receiver function	*DeShon and Schwartz* [2004]
Costa Rican margin	38–40	travel time, active	*Sallares et al.* [1999]
Nicaraguan margin	>40	travel time, active	*Walther et al.* [2000]
Average Costa Rica	34	travel time, passive	*Quintero and Kulhanek* [1998]
Central Costa Rica	32–36	travel time, passive	*Protti et al.* [1996]

band stations (BOA, HDC, JTS) supplement the TUCAN data.

[10] This study determines crustal structure from *SV* wavefields in the coda of the teleseismic *P* and *PP* waves. Teleseismic *PP* waves are included, as well as the *P* waves traditionally used in receiver function studies, to provide greater azimuthal coverage (Figure 2). All events with a body wave magnitude >5.0, and a signal-to-noise ratio >3 recorded by more than 10 stations per event are examined. Signals are also required to show a strong visual correlation between stations for a given event. These criteria give 59 earthquakes with useful signal, 30 with *P* signal and 29 with *PP*, to yield 1742 receiver functions, varying between 20 and 42 per station.

[11] The near-receiver scattered wavefield is calculated using the method of *Bostock and Rondenay* [1999], summarized here. First, all seismograms for each event are transformed into an up going wave vector (*P*, *SV*, *SH*) using the inverse free-surface transform [*Kennett*, 1991] for a 90 s window starting just before the *P* onset. This isolates the *P* from the scattered *SV* and *SH* components. Next, *P* components are aligned using multichannel cross correlation [*vanDecar and Crosson*, 1990] and the incident wavefield is calculated as the first eigenmode of the resulting wavefield image. This procedure minimizes noise in the estimated incident *P* wavefield, giving a more stable deconvolution than single-station deconvolution methods that is reliable to higher

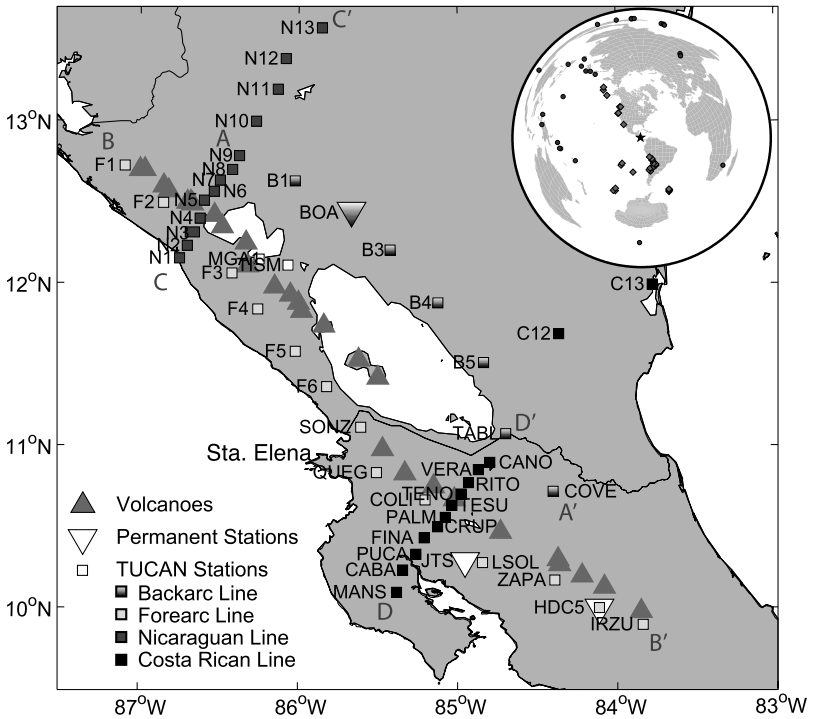

Figure 2. The TUCAN array in Central America. Squares represent temporary PASSCAL seismic stations, white inverted triangles represent permanent broadband stations, and triangles represent volcanoes. Inset shows map of events used; black star marks the center of the network, gray triangles show events providing *P* waves, and gray circles show events providing *PP* waves. Letters A-A′, B-B′, C-C′, and D-D′ show cross sections (Figures 5–8, 14).

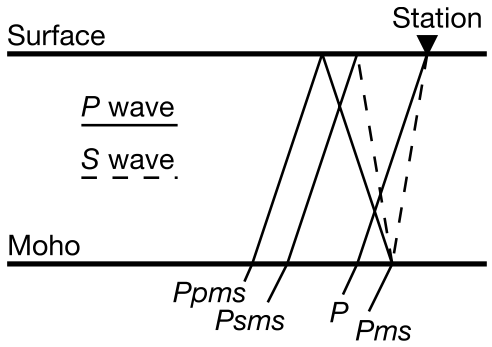

Figure 3. Ray geometry for primary converted phases analyzed here, from *Rossi et al.* [2006]. Moho conversion is denoted with "m."

frequencies [*Rondenay et al.*, 2005]. The incident *P* wavefield is deconvolved from each of the *SV* components for each station. The resulting scattered *SV* wavefield, here called receiver functions, comprise the basis of the data set used for all calculations and images.

[12] As a test, the *SH* wavefields are also processed. They show little to no energy for Moho conversions, so indicate that anisotropy or layer dip do not significantly affect signals.

3.2. Moveout Correction

[13] The arrival times of each converted phase at a given station are dependent on the incident ray parameter *p, Vp* and *Vs*, within the crust. A moveout correction is applied similar to *Rossi et al.* [2006], to convert time to depth for each event and converted phase *Ps*, *Ppms* and *Psms* (Figure 3), but is generalized here for arbitrary vertical velocity variations beneath each station. For a vertically stratified earth, the lag time of *Ps* after the *P* arrival is

$$t_{Ps-P} = \int_0^z \left(\sqrt{\frac{1}{v_s(z')^2} - p^2} - \sqrt{\frac{1}{v_p(z')^2} - p^2} \right) dz'$$

where $v_p(z)$ is the *P* velocity, $v_s(z)$ is the S velocity, p is the ray parameter and z is the layer thickness. Similar equations exist for *Ppms* and *Psms*. For a given velocity model ($v_s(z)$ and $v_p(z)$), these formulas describe an implicit monotonic dependence of layer depth, z, on phase lag time t_{Ps-P} (or t_{Ppms-P}, t_{Psms-P} for *Ppms* and *Psms*). These integrals are calculated numerically and inverted to give a moveout function converting lag time t_{Ps-P} to depth z.

3.3. Inversion for *Vp/Vs*

[14] The grid search method used to determine *Vp/Vs* for the crust follows *Rossi et al.* [2006] and is similar to *Zhu and Kanamori* [2000] and *Chevrot and van der Hilst* [2000]. The moveout correction is applied using a station-specific *Vp* model derived from tomography [*Syracuse et al.*, 2008]. Moveout-corrected records for the SV component are stacked over all events for a range of *Vp/Vs* from 1.5 to 2.2, at intervals of 0.01. Most stations are stacked over all events and phases (*Ps*, *Ppms*, *Psms*) weighted by stack variance, however in cases where signals could not be visually identified, only *Ps* and one of *Ppms* and *Psms* are used. Because there exist three possible significant conversions (*Ps*, *Ppms*, *Psms*), this leads to three estimates of signal amplitude as a function of depth, which should agree at the correct *Vp/Vs* (Figure 4a). Stack amplitudes should be highest at the depth of the dominant mode conversion and for the correct *Vp/Vs* (Figure 4b). It is assumed that the dominant mode conversion in the upper 50 km is the Moho.

[15] Best fitting *Vp/Vs* estimates vary strongly between adjacent stations, as found in other studies [*Rossi et al.*, 2006]. Since many raypaths are sampling similar crust at adjacent stations, there should be a smooth variation in *Vp/Vs* between stations, unlike what is observed. Hence, much of the local *Vp/Vs* variation must reflect measurement errors. To reduce the effect of this scatter, a 12-node 2-D spline surface is fit to the *Vp/Vs* estimates, and *Vp/Vs* on that surface is used rather than single station values. This procedure effectively reduces the number of free parameters describing *Vp/Vs*, to one per each four stations. Additionally, this procedure provides a robust *Vp/Vs* estimate for individual stations that varies smoothly.

3.4. Crustal Imaging

[16] Images are generated for each transect using moveout corrected stacks of the *Ps*, *Ppms* and *Psms* arrivals for the best fitting *Vp/Vs* for each station, as an estimate of structure vertically below each station. Along each transect, the stacked traces are collected, sorted and smoothed horizontally using a Gaussian filter with 10 km half width to suppress uncorrelated signal between adjacent stations [e.g., *Ferris et al.*, 2003]. Smoothing in this manner results in enhancement of subhorizontal layers, such as the Moho. Dipping slabs and complicated structure may be somewhat suppressed; in a test of this method in Alaska, moderate Moho and

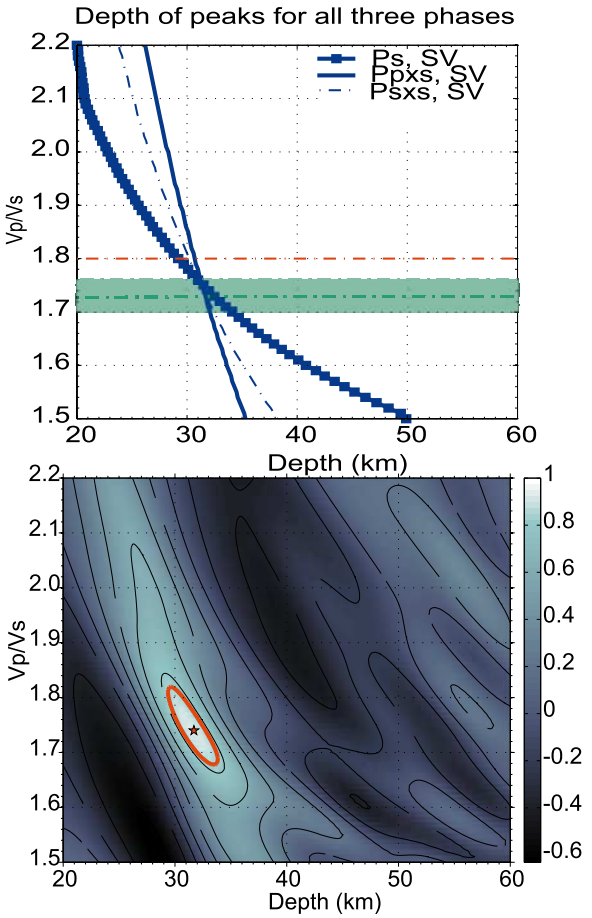

Figure 4. Crustal thickness and *Vp/Vs* inversion for station B3. (top) Tradeoff curve between crustal thickness and *Vp/Vs* for individual phases *Ps*, *Ppms*, and *Psms*, which agree at the correct *Vp/Vs*. Green line shows *Vp/Vs* from spline surface, with green bar showing 2-sigma uncertainty. Red dashed line shows *Vp/Vs* from tomography [*Syracuse et al.*, 2008]. (bottom) Amplitude of stack over all three converted phases, normalized to 1.0 at peak stack. The red contour marks the 85% confidence level from *t* test.

slab dips were recovered successfully [*Rossi et al.*, 2006]. In Central America a dipping subducting plate is not obvious in these images (discussed in section 4).

3.5. Formal Uncertainties

[17] Formal uncertainties for *Vp/Vs* are the predicted errors of the spline fit as discussed in section 3.5 and are typically ±0.04 (2-sigma from linear regression). Crustal thickness is calculated from stacks assuming these *Vp/Vs* values, including a 95% confidence limit based on a *t* test of stack amplitude variation [*Rossi et al.*, 2006]. The crustal thickness uncertainties (95% confidence level) are typically 2–4 km and range from 1.6 to 9.2 km (Table 2 and Figures 10 and 11). Actual uncertainties are somewhat larger because the estimates include several assumptions about velocities and structure; see section 5.

4. Results

4.1. Crustal Structure

[18] A stacked and moveout-corrected image of structure in the crust and upper mantle is generated for each of the along-arc and cross-arc lines (Figure 2). The transects show strong Moho signals in the back arc with weaker signals below the arc and along the fore arc. Internal crustal structure is generally simple in the back arc with more complicated structure beneath the arc and fore arc.

[19] The back-arc line reveals the simplest structure (Figure 5). It shows a strong Moho across the entire line with few other arrivals. A clear transition in *Vp/Vs* exists between B4 and B5. Crustal thickness varies from 30.6 ± 4.1 km to 31.7 ± 3.9 km from SE to NW, with the thinnest crust beneath Costa Rica, as *Vp/Vs* varies from 1.88 ± 0.14 to 1.75 ± 0.04 (Figure 5). The simplicity of this line shows that where structure is simple, clear Moho conversions are imaged. Any variations in strength of Moho from other portions of the arc can be interpreted as real features. It also shows that crust here is fairly homogenous away from the subduction zone.

[20] The fore arc shows a less clear Moho, with apparent steps and multiple interfaces imaged beneath some stations (Figure 6). A single, shallow interface underlies the Nicaragua fore arc between stations F3 and SONZ (28–36 km depth), and a deeper interface underlies much of the Costa Rica fore arc between COLI and IRZU (36–41 km depth). Both interfaces appear to both be present beneath QUEG in NW Costa Rica, with both depths shown in Table 2. This station is near the Santa Elena suture on the Pacific Coast (Figures 1 and 2) marking the northern boundary of basement with CLIP affinity [*Hauff et al.*, 2000], so the complex image may be due to the three-dimensional nature of this terrane boundary. Even away from this transition, crustal structure appears more complicated than in the back arc. Serpentinized mantle, fluids and melt all might effectively reduce the velocity contrast between crust and mantle, resulting in a reduction of the amplitude of the converted phases. However, as discussed in section 6.2, it is more likely that the complex Moho results

Table 2. Single-Station Inversion Results

Station	Longitude (deg)	Latitude (deg)	Elevation (km)	*Vp/Vs*[a]	Moho[a] (km)	*Vp*[b] (km/s)
B1	−86.021	12.632	0.435	1.75 ± 0.04[c]	31.7 ± 3.9	6.38
BOA	−85.666	12.449	0.381	1.75 ± 0.08[c]	31.9 ± 5.8	6.09
B3	−85.422	12.206	0.156	1.73 ± 0.06[c]	31.7 ± 2.2	6.12
B4	−85.122	11.881	0.107	1.74 ± 0.06[c]	33.6 ± 3.1[d]	6.27
B5	−84.836	11.514	0.062	1.84 ± 0.10[c]	31.8 ± 3.0[d]	6.39
TABL	−84.697	11.075	0.068	1.88 ± 0.08[c]	33.1 ± 1.7	6.01
COVE	−84.400	10.719	0.110	1.88 ± 0.14[c]	30.6 ± 4.1	6.33
N1	−86.750	12.155	0.024	1.77 ± 0.08[c]	31.6 ± 6.5	6.09
N2	−86.701	12.233	0.047	1.75 ± 0.06	28.5 ± 5.2/40.0 ± 3.3	5.99
N3	−86.645	12.307	0.068	1.74 ± 0.04[c]	26.5 ± 4.3/38.2 ± 2.8	5.93
N4	−86.621	12.401	0.065	1.73 ± 0.04	28.9 ± 6.4	6.01
N5	−86.594	12.511	0.106	1.72 ± 0.06[c]	24.6 ± 3.5[d]	6.27
N6	−86.532	12.566	0.108	1.71 ± 0.06	31.0 ± 2.1[d]	6.40
N7	−86.494	12.636	0.079	1.71 ± 0.06[c]	28.8 ± 1.8	6.28
N8	−86.417	12.701	0.141	1.72 ± 0.04[c]	31.4 ± 4.6	6.37
N9	−86.374	12.787	0.166	1.73 ± 0.04[c]	34.1 ± 3.2	6.46
N10	−86.268	12.999	0.620	1.75 ± 0.04[c]	39.5 ± 2.8	6.59
N11	−86.130	13.196	1.099	1.77 ± 0.06[c]	43.5 ± 2.5	6.61
N12	−86.081	13.385	0.804	1.75 ± 0.08[c]	35.8 ± 3.5	6.21
N13	−85.853	13.574	0.524	1.71 ± 0.16	36.0 ± 2.9	6.21
MANS	−85.381	10.099	0.119	1.73 ± 0.12[c]	27.2 ± 2.7	5.96
CABA	−85.343	10.236	0.042	1.71 ± 0.08	35.0 ± 2.0	6.18
PUCA	−85.260	10.333	0.041	1.71 ± 0.06	35.1 ± 2.2	6.04
FINA	−85.208	10.434	0.045	1.71 ± 0.04	33.2 ± 2.6	6.20
CRUP	−85.125	10.502	0.192	1.73 ± 0.04[c]	36.1 ± 2.1	6.59
PALM	−85.076	10.560	0.295	1.74 ± 0.02[c]	33.1 ± 5.1[d]	6.42
TESU	−85.035	10.634	0.772	1.76 ± 0.04	37.1 ± 4.8	6.52
TENO	−84.977	10.704	0.651	1.78 ± 0.04	37.9 ± 5.2[d]	6.52
RITO	−84.931	10.773	0.144	1.79 ± 0.04	33.1 ± 7.0[d]	6.32
VERA	−84.869	10.854	0.072	1.82 ± 0.04[c]	36.6 ± 3.6	6.30
CANO	−84.797	10.898	0.073	1.84 ± 0.06[c]	37.7 ± 3.0[d]	6.21
C12	−84.362	11.690	0.238	1.78 ± 0.08[c]	34.6 ± 2.8	6.48
C13	−83.772	11.994	0.037	1.69 ± 0.12[c]	36.0 ± 3.9[d]	6.28
F1	−87.096	12.725	0.139	1.72 ± 0.08[c]	31.8 ± 3.2[d]	6.25
F2	−86.853	12.497	0.144	1.74 ± 0.06[c]	38.4 ± 2.4[e]	6.62
F3	−86.419	12.064	0.250	1.72 ± 0.04[c]	35.9 ± 1.6	6.03
F4	−86.255	11.843	0.529	1.69 ± 0.04[c]	36.2 ± 2.9	6.55
F5	−86.019	11.582	0.107	1.66 ± 0.06[c]	26.0 ± 2.9	6.17
F6	−85.821	11.365	0.074	1.66 ± 0.08[c]	30.5 ± 3.1	6.18
SONZ	−85.607	11.115	0.148	1.67 ± 0.06[c]	28.2 ± 4.7	6.15
QUEG	−85.508	10.836	0.290	1.67 ± 0.06	30.3 ± 2.2/44.3 ± 3.9	6.26
COLI	−85.203	10.668	0.446	1.72 ± 0.04[c]	42.5 ± 2.3	6.62
LSOL	−84.843	10.282	1.075	1.80 ± 0.08	36.4 ± 2.0	6.22
ZAPA	−84.391	10.173	1.664	1.87 ± 0.12	40.0 ± 2.0	6.13
HDC5	−84.112	10.002	1.154	1.87 ± 0.08	37.0 ± 2.3[e]	6.26
IRZU	−83.839	9.898	1.812	1.85 ± 0.14[c]	40.5 ± 6.1	6.35
TISM	−86.067	12.113	0.114	1.69 ± 0.08	35.9 ± 3.5	6.21
JTS	−84.953	10.291	0.340	1.78 ± 0.06	41.0 ± 7.3	6.48
MGA1	−86.248	12.149	0.086	1.70 ± 0.04	27.7 ± 5.3	5.87

[a] Uncertainties are 2-σ for spline surface for *Vp/Vs*, or 95% from *t* test for Moho depth.
[b] Average *Vp* above Moho, using velocities from tomography [*Syracuse et al.*, 2008].
[c] Station *Vp/Vs* included in spline fit to calculate final *Vp/Vs*.
[d] Moho depth calculated from stack of *Ps* and *Ppms* for this station.
[e] Moho depth calculated from stack of *Ps* and *Psms* for this station.

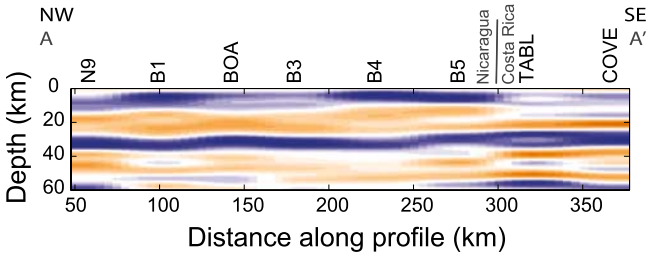

Figure 5. Receiver functions for back-arc line A-A′, stacked and interpolated as described in text. Orange shows positive conversions, and blue shows negative. Figure 2 shows line location.

from signal interferences within the crust, due to additional interfaces.

[21] The Nicaraguan cross-arc transect shows a clear Moho conversion in the back arc (Figure 7). Beneath the arc and fore arc, Moho conversions are more difficult to identify. In particular, stations N2 and N3 show two possible Moho conversions. The shallower depth allows for a continuous Moho through much of the transect and is consistent with initial migration results [*MacKenzie et al.*, 2007]; however, the deeper conversion has a higher stack amplitude. Thin crust beneath the arc is apparent, with crustal thickness varying from 31.6 ± 6.5 km at the trenchward end of the line to 24.6 ± 3.5 km beneath the arc, then increasing to a maximum of 43.5 ± 2.5 km in the Nicaragua Highlands back arc. The Wadati-Benioff Zone is approximately 90 km deep at the coastline (SW end of the line) and dips > 60°, so the slab is not imaged. A low-amplitude dipping structure lies below the Moho between the coast and arc, beneath the SW end of the line at 30 km depth and 60 km deep beneath the arc; a similar feature is imaged in refraction data (section 4.2).

[22] The Costa Rican transect shows a more complicated crustal structure than Nicaragua, particularly beneath the arc and fore arc (Figure 8). Additionally, the Moho is less clear throughout the line. Crustal thickness ranges from 27.2 ± 2.7 km at the southernmost fore-arc station to a maximum of 37.9 ± 5.2 km beneath the arc to 36.0 ± 3.9 km at the Caribbean coast. The dipping subducting slab is not clear in this image, although the Wadati-Benioff zone seismicity is 30 km deep at the SW end of the line, so it might be expected. This might be due to the nature of the smoothing as discussed in section 3.6, but preliminary tests (not shown) indicate the slab's absence is more likely due to defocusing due to the lack of migration, the subject of a follow-up study [*MacKenzie et al.*, 2007].

4.2. Comparison With Previous Studies

[23] Wide-angle refraction studies done in close proximity to each of the cross arc lines are in agreement with structure seen in receiver function images [*Sallares et al.*, 1999; *Walther et al.*, 2000]. The Costa Rican transect (Figure 8) structure matches in both the number and approximate locations of interfaces. Minor differences in the upper crust do exist, but are most likely a result of velocity model differences and resolution advantages an active refraction survey would have over receiver functions at depths <20 km. Wide-angle refraction studies in Nicaragua do not show Moho arrivals beneath land, leading those authors to infer that the Moho is >40 km deep [*Walther et al.*, 2000]. A dipping layer exists well above the expected subducting plate in the refraction study.

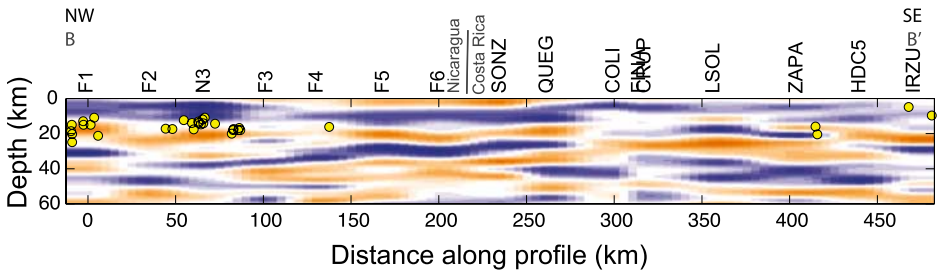

Figure 6. Interpolated receiver functions for fore-arc line B-B′. Format same as Figure 5. Yellow circles in this plot indicate seismicity near the section. Figure 2 shows line location.

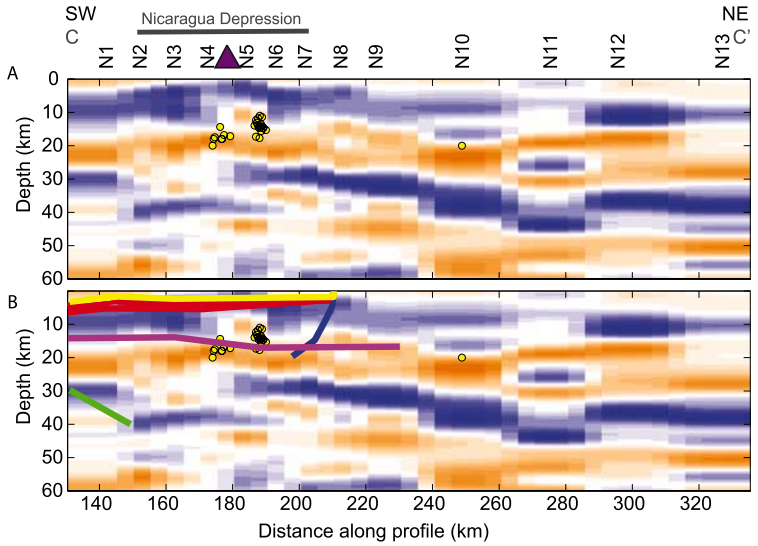

Figure 7. Interpolated receiver functions for Nicaraguan line C-C′; format same as Figure 5. Yellow circles in this plot indicate seismicity near section, and the purple triangle indicates the location of the arc. (a) Raw image. (b) Colored lines show interfaces from refraction survey [*Walther et al.*, 2000]. Figure 2 shows line location.

This dipping layer is consistent with the sub-Moho a boundary seen in the Nicaragua transect (Figure 7). Because of the horizontal smoothing, a dipping structure could appear step-like in our images. That feature was inferred by *Walther et al.* [2000] to be a relict suture from an older arc accretion event. If that interpretation is correct, then the boundary extends to 60 km depth, almost below the arc, and may extent as far north as station N9.

[24] *DeShon and Schwartz* [2004] found crustal models that could fit receiver functions for the Global Seismic Network station JTS with crustal thicknesses between 32 and 40 km, and a gradational Moho. Their corresponding average crustal velocities are Vp = 6.4–6.5 km/s and Vp/Vs = 1.78. Our results for JTS show a crustal thickness of 41.0 ± 7.3 km with a Vp/Vs of 1.78 ± 0.03, consistent with theirs within error bounds although somewhat thicker crust. It should be noted that this station has one of the largest uncertainties, which may account for this difference.

5. Other Sources of Uncertainties

5.1. Velocity Tradeoff

[25] A tradeoff exists between crustal thickness and velocity [*Ammon*, 1991], so any prior knowledge of the velocities reduces crustal thickness uncertainty. The velocity model used here, derived from tomography [*Syracuse et al.*, 2008], represents a best fit to travel time data. Attributing the entire root mean square residual from the tomographic inversion (0.22 s) to systematic local earthquake travel time errors in the crust leads to a ∼3% crustal thickness error, assuming near vertical rays. This translates into 1.7 km in crustal thickness error for typical thicknesses seen here (30–35 km). This calculation probably overestimates this effect, as it attributes all misfits of travel times to systematic crustal velocity errors. In reality some of the velocity misfits result from picking errors in the local earthquake travel times, and some come from elsewhere along the raypath.

[26] In another test of velocity sensitivities, all inversions were performed assuming constant crustal velocity of 6.5 km/s, rather than velocities derived from tomography. Stack amplitudes of the Moho conversion using the tomographic velocity model are 23.4% higher than those in this test, indicating that the tomographically derived velocities describe phase moveout more accurately. In other words, the receiver functions show sensitivity to the velocities used; the velocities-thickness tradeoffs are not total [*Ammon*, 1991].

5.2. Azimuthal Variation

[27] Azimuthal variations in estimated crustal thickness may exist in the presence of dipping layers or anisotropy, possibly leading to overestimation or underestimation of crustal thickness [*Cassidy*, 1992]. In order to ensure that these effects are small, traces are stacked separately for different back azimuth ranges and compared. Fig-

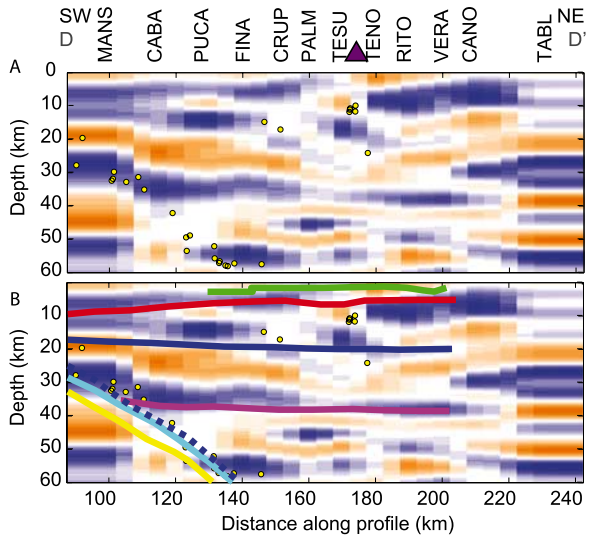

Figure 8 Interpolated receiver functions for Costa Rican line D-D′. Format same as Figure 7. (a) Raw image. (b) Colored lines show main interfaces from refraction survey [*Sallares et al.*, 1999]. Figure 2 shows line location.

ures 9a and 9b show strong similarity in structure for various back azimuth coverage. The correlation coefficient, *R,* between images for the back azimuth ranges from 320 to 45° and from 135 to 230° is 0.84, indicating good agreement for Moho structure.

[28] Processing of *SH* receiver functions confirms minimal dip and anisotropy. These signals lack a clear signal from Moho conversions. This indicates that the effects of a dipping Moho and anisotropy do not affect results.

5.3. Distance and Phase Type

[29] This study uses *P* and *PP* arrivals for receiver functions. The *PP* signals are more attenuated than *P*, and lower in frequency content. To ensure the differences between *P* and *PP* arrivals do not bias images, traces are stacked separately for these two phases (Figures 9c and 9d). The correlation coefficient, *R*, between images for the *P* and *PP* stack is 0.51. Most differences lie in the complex subarc Moho, and most other parts of the image are quite similar.

5.4. Near-Surface Layer and Forward Modeling

[30] Strong positive arrivals at <1.5 s after the *P* arrival indicate a slow layer across much of the network (Figures 5–8). It has been shown that a low-velocity near-surface layer introduces a phase delay in waves passing through the basin that can interfere with *Ps* [e.g., *Sheehan et al.*, 1995]. Here, sediments in the Nicaragua Depression, and widespread volcaniclastic deposits and Cretaceous-Eocene marine sediments [*McBirney and Wiliams*, 1965; *Ranero et al.*, 2000] underlie most stations. A sedimentary layer or layer of slow volcanics is consistent with a low-velocity upper layer in refraction studies by *Sallares et al.* [1999] in Nicaragua and *Walther et al.* [2000] in Costa Rica. Both observed a <5 km thick layer with velocities of 2–4 km/s. Gravity modeling indicates 2.5 km of sediment and volcaniclastics [*Elming and Rasmussen*, 1997].

[31] Synthetic receiver functions generated without a layer of sediment show simple patterns (Figure 10a). The stack of *Ps*, *Ppms* and *Psms* generates a small pulse at <10 km depth and also adds side lobes to the stacked Moho conversion not seen in *Ps*. These lobes are <30% of the amplitude of the stacked arrival, so features <30% of the main picks should be interpreted with caution.

[32] Station B3 is representative of stations outside of the Nicaragua depression (Figure 10b). A 2 km

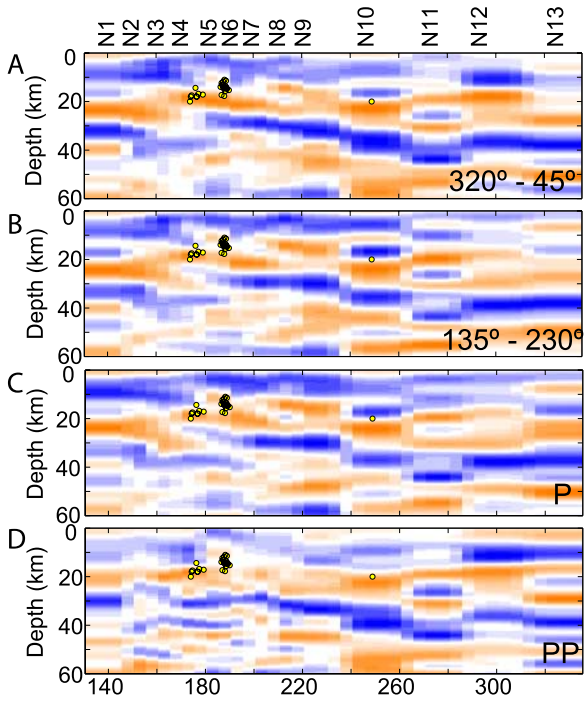

Figure 9. Nicaraguan transect imaged with different subsets of data. (a) Events from 320 to 45° back azimuth. (b) Events from 135 to 230°. (c) *P* arrivals only. (d) *PP* arrivals only.

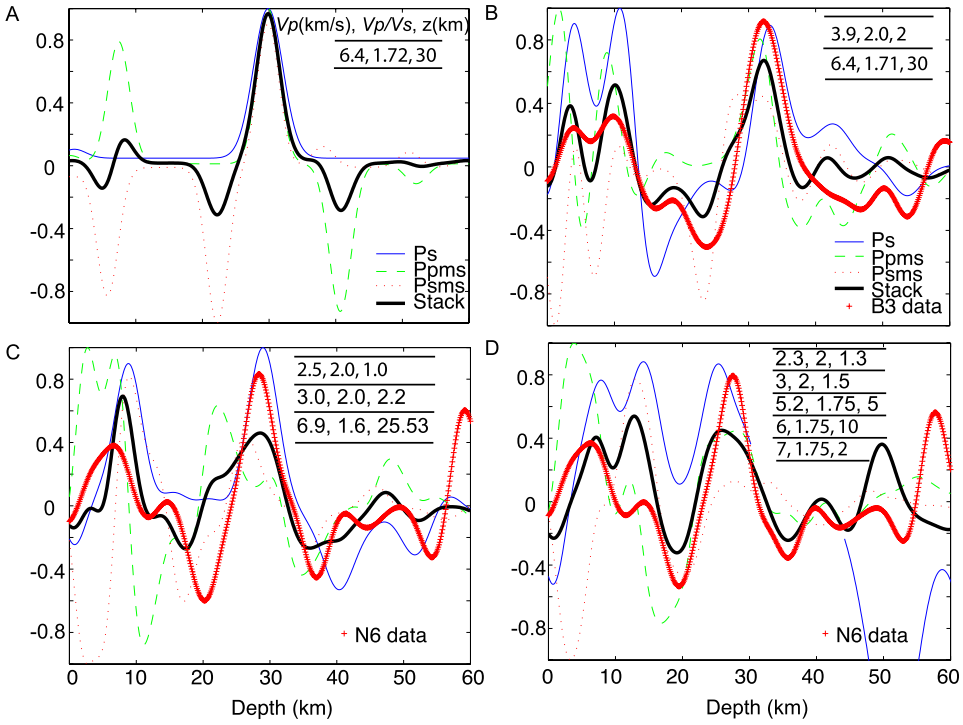

Figure 10. Forward modeling of receiver function stacks. Thick black lines are calculated and the red lines are observed receiver function stacks for sample stations; individual modes (*Ps, Ppms, Psms*) are also shown. (a) Synthetics generated for a single-layer crust (Vp = 6.4 km s^{-1}) illustrating the contributions of different modes. (b) Synthetics generated for a crust with a single slow surface layer, compared with station B3 representing typical back arc. (c) Synthetics generated for a crust with two slow surface layers, compared with data from station N6, representative of stations within the Nicaraguan Depression. (d) Synthetics derived from more complex model of *Walther et al.* [2000] compared with Nicaragua Depression station N6.

thick low-velocity layer overlying a 28 km thick crust generates signals similar to those observed, matching arrival times of primary peaks (velocities shown on Figure 10). Amplitudes are not matched perfectly because we assume the crystalline crust has constant velocity, not a gradient, giving higher velocity contrast at the basin bottom than are likely to be present. Additionally, all phases in the synthetic stack are weighted equally whereas the data stack weighting is dependent upon the stack coherence [*Rossi et al.*, 2006].

[33] Synthetic seismograms generated without a sedimentary layer (Figure 10a) show no bias, or depth difference between phases, in Moho conversions. A shift in estimated Moho depth of ~0.1 km exists because of velocity model differences between those used to generate synthetics and in applying the moveout correction to the synthetics. However, synthetic data that include a 2 km low-velocity layer show a bias in arrivals of Moho conversions (Figure 10b). The direct *Ps* conversion shows the greatest bias with a ~1.2 km overestimate in depth, but stacking over all three phases (*Ps*, *Ppms* and *Psms*) reduces the overestimation due to a sedimentary basin to <0.3 km. Synthetic stacks that include a sediment layer show greater complexity and interferences.

[34] Station N6 typifies stations within the Nicaragua Depression (Figure 10c). Forward modeling of these receiver functions shows that good fits require two slower layers, each ~1.5 km thick with velocities of ~2.5 and 3 km/s. Neglecting them would result in a <0.3 km bias in the Moho depth estimate. Addition of midcrustal layers reduces the impedance contrast between layers, more accurately representing amplitudes (Figure 10d).

5.5. Summary

[35] All tests discussed here contribute to the uncertainty in crustal thickness. All stations sit upon at least one layer of slow sediments and volcanics, except perhaps one or two stations on crystalline basement of the Nicoya Peninsula, Costa Rica, producing secondary signals. Combining

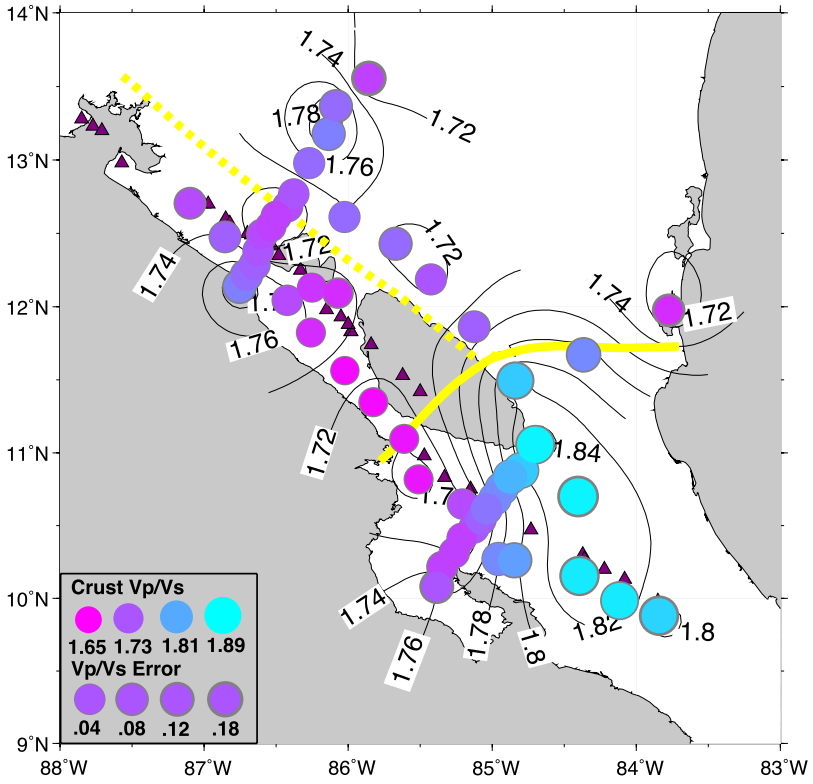

Figure 11. *Vp/Vs* for each station, indicated by size and color of symbols. The size of the gray border indicates 2-σ uncertainty on each measurement.

uncertainties due to the velocity model with basin effects produces an additional uncertainty of 1.5–2.0 km for all stations in addition to formal errors. The formal errors generally exceed this additional uncertainty, so describe uncertainties well (Table 2).

6. Discussion

6.1. Terrane Boundaries

[36] Terrane boundaries separate the three major blocks that compose northern Costa Rica and Nicaragua. The exact locations of these boundaries are unclear in large part because of the widespread volcanic cover. However, along the back-arc line a clear transition in *Vp/Vs* occurs between stations B4 and B5 (Figure 11), along with a subtle change in crustal structure (Figure 5). This transition is a good candidate for the Chortis-Chorotega terrane boundary, thought to lie somewhere nearby [e.g., *Case et al.*, 1990; *Mann et al.*, 2007]. Lower *Vp/Vs* estimates (1.71–1.77) exist to the northwest, consistent with a silicic continental crust, while the southeast part of this transect shows *Vp/Vs* of 1.82–1.88, consistent with mafic compositions expected for the Caribbean Large Igneous Province (CLIP) thought to represent Chorotega basement (Figure 11) [e.g., *Ball et al.*, 1969; *Pindell and Dewey*, 1982; *Sinton et al.*, 1997; *von Huene and Scholl*, 1991]. A compositional change is required to account for the change in *Vp/Vs*, with more mafic *Vp/Vs* to the SE, leading us to infer the terrane boundary lies between the stations. The boundary shows slight offsets of the Moho, perhaps indicating an imbricated terrane boundary. Thus, the CLIP basement extends throughout Costa Rica and is not just limited to exposures along the Pacific coast. The Moho step would place that boundary in the lowlands just north of the Nicaragua-Costa Rican border (Figure 1).

[37] A second boundary should exist in the fore arc near the Pacific Coast between the accreted coastal terrane to the north and Chorotega block. A transition in both crustal thickness (Figure 6) and *Vp/Vs* (Figure 11) indicates that the boundary lies somewhere between stations SONZ and COLI, or near the Santa Elena Peninsula ophiolite. Station QUEG lies between SONZ and COLI and shows two distinct possibilities for crustal thickness, each possibility corresponding to adjacent stations SONZ and COLI, possibly an effect of the three-

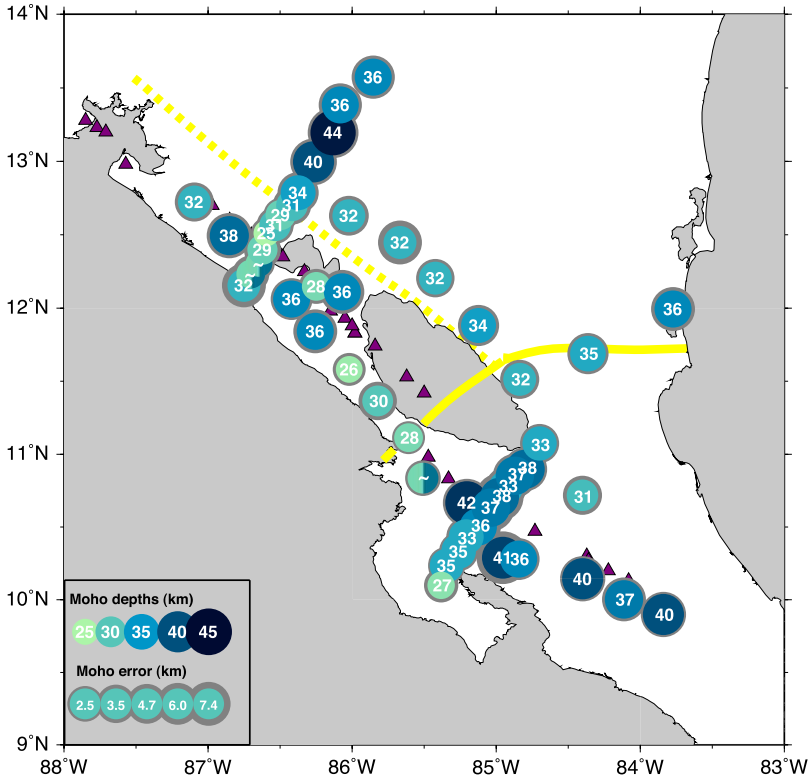

Figure 12. Crustal thickness below each station, marked by color and size of circles. Uncertainty on crustal thickness is marked by the size of the gray band around circle. Uncertainty includes formal 95% confidence interval increased to account for issues discussed in section 5.

dimensional nature of this transition. The Santa Elena ophiolite is chemically distinct from CLIP provenance basalts further SE and may represent an exposure of an older arc accreted to North America [*Hauff et al.*, 1997; *Meschede and Frisch*, 1998; *Walther et al.*, 2000]. Thus, the boundary between the Santa Elena arc basement and the Nicoya oceanic plateau basement extends through the crust in this region.

[38] The third boundary expected, between the Nicaragua accreted arc terrane and the Chortis block is not obvious from these data. It probably lies near the modern Nicaragua arc and follows it, where the Nicaragua Depression complicates crustal structure. However, some complications seen in signals may be due to this suture, discussed below.

6.2. Arc and Fore-Arc Crustal Structure

[39] The back arc, including regions beneath the Miocene arc of Nicaragua, shows a clear Moho and simple crustal structure (Figures 5, 7, and 8). Beneath the modern arc and fore arc, images show complicated structure and a reduction in Moho conversion strength (Figures 7 and 8). Serpentinized mantle, fluids, mafic cumulates and melt all could reduce the velocity contrast between crust and mantle, and could result in a reduction of the amplitude of the converted phases beneath the arc and in the fore arc [e.g., *Behn and Kelemen*, 2006; *Hyndman and Peacock*, 2003]. Both cross arc transects show a clear reduction in signal directly beneath the arc, consistent with these effects. However, because of many signal corrections done in the stacking to enhance phase accuracy, the true conversion amplitudes cannot be directly inferred from images.

[40] To understand the nature of these conversions, the original *SV* traces are restacked without normalization at the best fitting *Vp/Vs,* selecting only those signals with the highest signal-to-noise ratios and removing outliers. The traces give amplitudes of *SV* waves such as *Ps*, *Ppms*, and *Psms* relative to the incident *P* wave, with free surface effects removed [*Bostock and Rondenay*, 1999]. Moho conversion amplitudes show no clear difference between fore-arc and back-arc stations, and both show Moho conversions with average amplitudes of 0.13 for *Ps* and 0.08 for *Ppms*. Forward mod-

eling indicates that sediment layers interfere with the *Ps* arrival so that amplitude can be biased, however *Ppms* arrives later than most sediment reverberations, so their amplitudes should better indicate velocity contrasts. The *Ppms* amplitudes require a velocity contrast of 0.5–1.0 km/s according to synthetic receiver functions processed in the same manner to actual data, with identical amplitude renormalization. Stronger amplitudes are present directly beneath the arc in both Costa Rica and Nicaragua, 0.24 and 0.15 for the *Ps* and *Ppms* conversions respectively. The signal-to-noise ratio for these stations is not significantly different from the rest of the network, so the high amplitude may be due large velocity contrasts perhaps associated with melt-rich layers. In general, strong velocity contrasts persist under arc and fore arc, so that if crustal mafic cumulates or slow mantle serpentine exist, they have a minimal effect on velocities. Rather, images are affected by interferences of other crustal phases.

[41] In the fore arc, complicated structure shows multiple, discontinuous interfaces. Complicated structure in these images may result from out of plane conversions from dipping layers. Such structure is expected for this region since the fore-arc terrane boundaries intersect the arc obliquely (Figure 1), at unknown dip. Such geometry may give rise to the discontinuous Moho observed near the Santa Elena suture (Figure 6).

6.3. Thin Crust Beneath the Nicaragua Arc

[42] Crust is 11–18 km thinner in the center of the Nicaragua Depression than the Highlands 100 km to the northeast (Figures 7 and 12). Here we examine if the thin crust is a result of crustal extension. To accommodate 11–18 km of crustal thinning by extension, simple crustal stretching calculations [*McKenzie*, 1978] suggest that 3.4–8.1 km of syn-rift sediment should be present, or 4.7–9.4 km including later thermal subsidence. Sediment thickness in the Depression has not been directly measured, but estimated at 2–2.5 km from potential field data [*Elming and Rasmussen*, 1997], consistent with thicknesses of late Cretaceous-Eocene marine section seen in the adjacent coastal hills [*Ranero et al.*, 2000]. Similarly, receiver functions show a signal from the base of a shallow low-velocity layer best modeled as 3.2 km of sediments (Figure 10c). Thus, the basin appears to be far too shallow to isostatically balance the changes in crustal thickness; it also has a quite different geometry. Gradually increasing crustal velocities from the arc to the northeast (Table 2) indicate that changes in crustal density might isostatically compensate the changes in crustal thickness, as do more detailed buoyancy calculations (section 6.5).

[43] It is unclear that crustal thinning represents a geologically recent phenomenon, and several indicators suggest relatively little extension since the Plio-Pleistocene arc formed, even though the Depression also formed at that time [*Weinberg*, 1992]. Current GPS measurements show that the fore arc is translating NW at 15 mm/a with only a few mm/a at most of arc-normal extension [*Turner et al.*, 2007], and may be accommodated by bookshelf-type faulting on arc-normal strike-slip fault systems [*La Femina et al.*, 2002] which would lead to little crustal thinning. There is also very little recent basin subsidence; borehole data shows less than 150 m of Quaternary volcaniclastic sediment overlying Tertiary ignimbrites near the Nicaragua transect [*van Wyk de Vries*, 1993]. The main evidence for large Neogene stretching comes from the distribution of Miocene volcanic arc rocks. Most Miocene (7–25 Ma) volcanics lie to the northeast of the Depression, but the Tamarindo volcanics (14–18 Ma) lie on the western coastal hills; both belts follow many of the same geochemical trends as the modern arc so may have been contiguous [*Balzer*, 1999; *Plank et al.*, 2002]. The simplest reconstruction of the arc would require complete opening of the 50 km wide Depression since the youngest Tamarindo volcanics formed (~14 Ma). It is not clear how to reconcile this observation with the lack of obvious fill in the Depression; perhaps the two suites of volcanics have different origins, as reflected by some geochemical proxies [*Saginor*, 2007; T. Plank, personal communication, 2007]. Regardless, the lack of significant potential field anomalies expected from a thick basin [*Elming and Rasmussen*, 1997] indicates that rifting does not explain well the crustal geometry. Possibly, the westward decrease in crustal thickness represents the fore-arc geometry prior to the postulated early Tertiary collision [*Walther et al.*, 2000].

[44] If the crustal structure predates the Depression and the modern volcanic arc, then the thin crust may have localized both features. Such thin crust forms an obvious site for deformation to concentrate, for example to form the Depression. More speculatively, magmas ascending to the modern arc may focus from the site of their generation to the thinnest crust, rather than rising vertically from

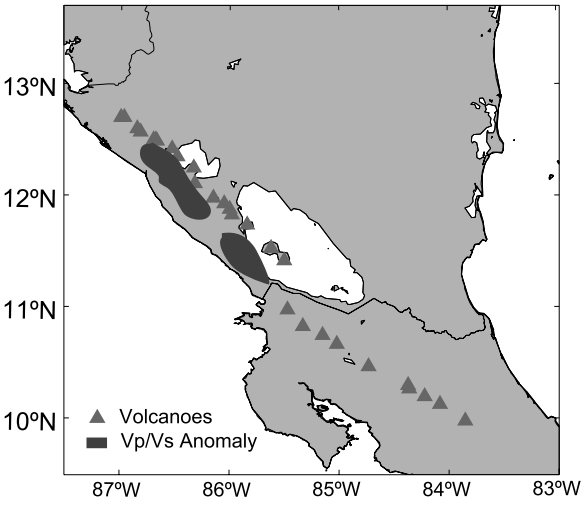

Figure 13. Outline of Vp/Vs anomaly in tomography at 80 km depth [*Syracuse et al.*, 2008].

their source. Seismic tomography [*Syracuse et al.*, 2008] show a sheet of high *Vp/Vs* extending vertically from slab to arc in Nicaragua, a potential proxy for melt [*Hammond and Humphreys*, 2000; *Takei*, 2002]. At 80 km depth the *Vp/Vs* anomaly lies just west of the front and is not quite parallel to it; in northwest Nicaragua it lies under the arc, but at the farther southeast end it lies 40–50 km trenchward, aligned with the location of the arc front in Costa Rica (Figure 13). This indicates that between 80 km depth and the surface the location of the magma is shifting toward the thinnest crust in southern Nicaragua, rather than ascending vertically.

6.4. Isostasy and Lithosphere

[45] It is probable that mantle thermal structure (lithosphere thickness) plays a role in arc plumbing. We estimate the mantle contribution to lithosphere buoyancy, assuming simple local isostatic compensation below each seismograph. Mantle residual elevation (*Hm*) can be defined as $Hm = e - [(\rho_a - \rho_c/)\rho_a]L_c + H_0$, where e is (subarial) elevation, L_c is the measured crustal thickness, ρ_a and ρ_c are the asthenospheric and crustal densities respectively, and H_0 is the reference elevation of an asthenospheric column (−2.4 km) [*Lachenbruch and Morgan*, 1990]. Figure 14 shows *Hm* for the Costa Rica and Nicaragua transect; here, we derive ρ_c from the average crustal *Vp* of Table 2 with *Brocher* [2005, equation 1], and set ρ_a = 3200 kg m^{-3}. One interpretation of H_m is that it reflects replacement of asthenosphere by high-density lithosphere, so we also calculate nominal lithosphere thickness $Lm = [\rho_a/(\rho_a - \rho_m)]Hm$, where ρ_m is the mantle lithosphere density (assumed to be 3250 kg m^{-3}). *Lm* is more subject to systematic errors than *Hm,* but it is more intuitively understandable. Even assuming $\rho_a - \rho_m$ is correct, uncertainties in *Lm* are of the order 25–40 km, stemming from uncertainties in L_c and ρ_c.

[46] The cross sections (Figure 14) show two trends. First, the thinnest lithosphere lies directly beneath the arc, increasing rapidly trenchward with similar thicknesses along both sections. While the trenchward increase may be influenced by other forces such as elastic flexure, the pattern does suggest that the lithosphere thins rapidly toward the active arc, qualitatively consistent with temperature variations inferred from seismic attenuation [*Rychert et al.*, 2008]. Second, the back arc in Nicaragua shows generally hot mantle (thin lithosphere) for 100 km behind the arc despite the large change in crustal thickness. The small change in *Hm* in most of the Nicaragua back arc demonstrates that the changes in crustal thickness are compensated by changes in crustal density over this interval. A thick lithospheric root beneath the low-elevation Costa Rica back arc appears required by these calculations; however, ρ_c may be underestimated in Costa Rica, as the low back arc *Vp* (6.1–6.4 km s^{-1}) seems inconsistent with the inference of CLIP basement made from geology and *Vp/Vs*. Still, these comparisons of elevation to crustal thickness suggest that the Costa Rica back-arc mantle may be significantly colder than that beneath Nicaragua.

6.5. Crustal Thickening and Continental Growth

[47] Continents grow in part through magmatic addition at volcanic arcs [e.g., *McLennan and Taylor*, 1982; *Taylor*, 1977; *Taylor and McLennan*, 1981]. The thick crust beneath the Costa Rica arc may reflect such magmatic addition [e.g., *Carr et al.*, 2007]. To test this hypothesis, crustal growth rates are calculated by estimating a crustal thickness at the onset of magmatism, calculating the difference in volume between the starting crustal thickness and present-day observed crustal thickness, and dividing this by the time over which the arc was active [*Reymer and Schubert*, 1984]. Elsewhere, typical crustal growth rates range from 10 to 82 km^3/km/Ma [*Holbrook et al.*, 1999; *Reymer and Schubert*, 1984; *Suyehiro et al.*,

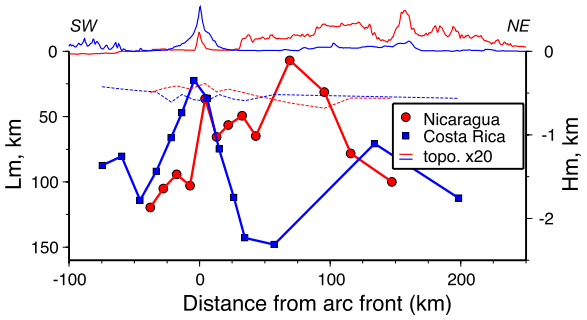

Figure 14. Mantle residual elevation (*Hm*) and nominal lithosphere thickness (*Lm*) across the two arc-normal sections. Sections aligned on nearest arc volcano as 0 km. *Hm* and *Lm* derived from crustal thickness, elevation, and velocity, as described in text following *Lachenbruch and Morgan* [1990]. Thin solid lines show elevation along each section, and thin dashed lines show crustal thickness (Table 1) at same scale as *Lm*; note, however, that *Lm = 0* corresponds to base not top of crust. Nicaragua profile is denoted by red lines, and Costa Rica is denoted by blue lines. Uncertainties in *Lm* due to formal errors in crustal thickness are 20–30 km.

1996; *Taira et al.*, 1998]. For Costa Rica the 32 km back-arc crustal thickness serves as an approximate premagmatic thickness, and magmatism started at 22 Ma [*Gazel et al.*, 2005], giving a crustal growth rate of 10.2 km^3/km/Ma, at the low end of other estimates. However, this is very sensitive to the age and crustal thickness at magmatic onset. Decreasing the initial crustal thickness to 30 km gives 23.2 km^3/km/Ma. While there is much uncertainty in the geometry of the prearc crust, the general consistency of rates calculated here with the lowest estimates from other arc indicate that Moho topography in Costa Rica could be explained by magmatic addition with the possible loss of volume through foundering of the lower crust [*Jull and Kelemen*, 2001; *Kay and Kay*, 1986]. The thin crust and young arc in Nicaragua precludes similar analysis there.

7. Conclusions

[48] Crustal thickness under the TUCAN array ranges from 26 to 42 km over just a few tens of kilometers. The crust is thicker in the center of the fore arc than toward the ends of this transect and in the back arc. The back-arc line exhibits a constant crustal thickness of 32–34 km. The thickest crust seen in the network lies beneath the highlands in Nicaragua (43.5 ± 2.5 km) and beneath the arc in Costa Rica (37.9 ± 5.2). The thinnest crust is seen directly beneath the arc in the Nicaragua Depression (24.6 ± 3.5 km), where the modern arc is located. The contrast between thick crust under the Costa Rica arc and thin crust under the Nicaragua arc represents a first-order contrast between these arc segments.

[49] Two distinct boundaries are seen marking the bounds of the coastal accreted terrane of Nicaragua with the Chortis and Chorotega blocks. Both boundaries are significant features that extend through the entire crust, showing that the terranes are not thin near-surface slivers. They separate regions of differing crust-averaged *Vp/Vs* and different discontinuity structure. Seismically imaging this region has delineated these boundaries beneath widespread volcanic cover.

[50] The location of the modern arc in Nicaragua is focused to the thinnest crust in the Nicaragua Depression. Crustal thinning appears to predate the arc and be isostatically compensated by changes in crustal density, but a thick rift basin is absent. Thinning of mantle lithosphere is also inferred beneath the arc, consistent with this speculation. A shift in tomographic high-*Vp/Vs* anomalies from 80 km depth to the surface in Nicaragua is interpreted as evidence that focusing of melt is somehow controlled by crustal structure.

[51] Crustal structure in most of the region shows a layer of sediment and/or slow volcanics in the upper few km. A simple structure exists in the back arc, with a complicated structure in the fore arc. Moho conversions show no difference in amplitude between the fore arc and back arc for each cross arc transect, indicating strong velocity contrasts between the crust and mantle with a minimal effect from serpentization of the mantle wedge or fast material accumulating at the base of the crust. Overall, these images reveal a complex interplay between magmatism and tectonics beneath this quasi-continental arc, ultimately producing a seismically simple structure after magmatism has ceased.

Acknowledgments

[52] We thank the large group who made the TUCAN data collection possible: P. Peres and A. Morales and many others at INETER; J. Pacheco at OVSICORI; T. Parker, N. Barstow, and others from the PASSCAL Instrument Center; D. Abt, C. Rychert, A. Walker, and M. Salas at Brown; and G. Reyes at B.U. A. Ferris, G. Rossi, and S. Rondenay provided assistance with early stages of the analysis. We thank S. Rondenay for making his preprocessing codes available. This work benefited from thoughtful reviews from Michael Carr and Eli Silver, as

well as discussions with numerous participants at the 2007 MARGINS-SFB574 Central America workshop. This work is supported by National Science Foundation grant OCE-0203650.

References

Ammon, C. J. (1991), The isolation of receiver effects from teleseismic P-wave-forms, *Bull. Seismol. Soc. Am.*, *81*, 2504–2510.

Ball, M. M., C. G. A. Harrison, and P. R. Supko (1969), Atlantic opening and origin of Caribbean, *Nature*, *223*, 167–168, doi:10.1038/223167a0.

Balzer, V. G. (1999), The late Miocene history of sediment subduction and recycling as recorded in the Nicaraguan volcanic arc, M.S. thesis, Univ. of Kans., Lawrence.

Barckhausen, U., C. R. Ranero, R. von Huene, S. C. Cande, and H. A. Roeser (2001), Revised tectonic boundaries in the Cocos Plate off Costa Rica: Implications for the segmentation of the convergent margin and for plate tectonic models, *J. Geophys. Res.*, *106*, 19,207–19,220.

Baumgartner, P. O., and P. Denyer (2006), Evidence for middle Cretaceous accretion at Santa Elena Peninsula (Santa Rosa Accretionary Complex), Costa Rica, *Geol. Acta*, *4*, 179–191.

Behn, M. D., and P. B. Kelemen (2006), Stability of arc lower crust: Insights from the Talkeetna arc section, south central Alaska, and the seismic structure of modern arcs, *J. Geophys. Res.*, *111*, B11207, doi:10.1029/2006JB004327.

Bostock, M. G., and S. Rondenay (1999), Migration of scattered teleseismic body waves, *Geophys. J. Int.*, *137*, 732–746, doi:10.1046/j.1365-246x.1999.00813.x.

Brocher, T. M. (2005), Empirical relations between elastic wavespeeds and density in the Earth's crust, *Bull. Seismol. Soc. Am.*, *95*, 2081–2092, doi:10.1785/0120050077.

Burbach, G. V., C. Frohlich, W. D. Pennington, and T. Matumoto (1984), Seismicity and tectonics of the subducted Cocos Plate, *J. Geophys. Res.*, *89*, 7719–7735, doi:10.1029/JB089iB09p07719.

Carr, M. (1984), Symmetrical and segmented variation of physical and geochemical characteristics of the Central American volcanic front, *J. Volcanol. Geotherm. Res.*, *20*, 231–252, doi:10.1016/0377-0273(84)90041-6.

Carr, M. J., I. Saginor, G. E. Alvarado, L. L. Bolge, F. N. Lindsay, K. Milidakis, B. D. Turrin, M. D. Feigenson, and C. C. Swisher III (2007), Element fluxes from the volcanic front of Nicaragua and Costa Rica, *Geochem. Geophys. Geosyst.*, *8*, Q06001, doi:10.1029/2006GC001396.

Case, J. E., W. D. MacDonald, and P. J. Fox (1990), Caribbean crustal provinces; seismic and gravidy evidence, in *The Caribbean Region. The Geology of North America*, edited by G. Dengo and J. E. Case, pp. 15–36, Geol. Soc. of Am., Boulder, Colo.

Cassidy, J. (1992), Numerical experiments in broadband receiver function analysis, *Bull. Seismol. Soc. Am.*, *82*, 1453–1474.

Chevrot, S., and R. D. van der Hilst (2000), The Poisson ratio of the Australian crust: Geological and geophysical implications, *Earth Planet. Sci. Lett.*, *183*, 121–132, doi:10.1016/S0012-821X(00)00264-8.

Dengo, G. (1985), Mid-America: Tectonic settings for the Pacific margin from southern Mexico to Colombia, in *The Ocean Basins and Margins*, edited by A. Nairn et al., pp. 123–180, Plenum, New York.

DeShon, H. R., and S. Y. Schwartz (2004), Evidence for serpentinization of the forearc mantle wedge along the Nicoya Peninsula, Costa Rica, *Geophys. Res. Lett.*, *31*, L21611, doi:10.1029/2004GL021179.

Ehrenborg, J. (1996), A new stratigraphy for the Tertiary volcanic rocks of the Nicaraguan highland, *Geol. Soc. Am. Bull.*, *108*, 830–842, doi:10.1130/0016-7606(1996)108<0830:ANSFTT>2.3.CO;2.

Elming, S. A., and T. Rasmussen (1997), Results of magnetotelluric and gravimetric measurements in western Nicaragua, central America, *Geophys. J. Int.*, *128*, 647–658, doi:10.1111/j.1365-246X.1997.tb05326.x.

Ferris, A., G. A. Abers, D. H. Christensen, and E. Veenstra (2003), High resolution image of the subducted Pacific (?) plate beneath central Alaska, 50–150 km depth, *Earth Planet. Sci. Lett.*, *214*, 575–588, doi:10.1016/S0012-821X(03)00403-5.

Gazel, E., G. Alvarado, J. Obando, and A. Alfaro (2005), Geologica y evolucion magmatica del arco de Sarapique, Costa Rica, *Rev. Geol. Am. Cent.*, *32*, 13–31.

Hammond, W. C., and E. D. Humphreys (2000), Upper mantle seismic wave velocity: Effects of realistic partial melt geometries, *J. Geophys. Res.*, *105*, 10,975–10,986.

Hauff, F., K. Hoernle, H. U. Schmincke, and R. Werner (1997), A Mid Cretaceous origin for the Galapagos hotspot: Volcanological, petrological and geochemical evidence from Costa Rican oceanic crustal segments, *Geol. Rundsch.*, *86*, 141–155.

Hauff, F., K. Hoernle, G. Tilton, D. W. Graham, and A. C. Kerr (2000), Large volume recycling of oceanic lithosphere over short time scales: Geochemical constraints from the Caribbean Large Igneous Province, *Earth Planet. Sci. Lett.*, *174*, 247–263, doi:10.1016/S0012-821X(99)00272-1.

Hoernle, K., P. van den Bogaard, R. Werner, B. Lissinna, F. Hauff, G. Alvarado, and D. Garbe-Schonberg (2002), Missing history (16–71 Ma) of the Galpapagos hotspot: Implications for the tectonic and biological evolution of the Americas, *Geology*, *30*, 795–798, doi:10.1130/0091-7613(2002)030<0795:MHMOTG>2.0.CO;2.

Holbrook, W. S., D. Lizarralde, S. McGeary, N. Bangs, and J. Diebold (1999), Structure and composition of the Aleutian island arc and implications for continental crustal growth, *Geology*, *27*, 31–34, doi:10.1130/0091-7613(1999)027<0031:SACOTA>2.3.CO;2.

Hyndman, R. D., and S. M. Peacock (2003), Serpentinization of the forearc mantle, *Earth Planet. Sci. Lett.*, *212*, 417–432, doi:10.1016/S0012-821X(03)00263-2.

Jull, M., and P. B. Kelemen (2001), On the conditions for lower crustal convective instability, *J. Geophys. Res.*, *106*, 6423–6446.

Kay, S. M., and R. W. Kay (1986), Petrology and gochemistry of the lower continental crust: An overview, in *The Nature of Lower Continental Crust*, edited by J. B. Dawson et al., pp. 147–159, Geol. Soc., London.

Kennett, B. L. N. (1991), The removal of free-surface interactions from 3-component seismograms, *Geophys. J. Int.*, *104*, 153–163, doi:10.1111/j.1365-246X.1991.tb02501.x.

Klemperer, S. L. (1989), Deep seismic-reflection profiling and the growth of the continental-crust, *Tectonophysics*, *161*, 233–244, doi:10.1016/0040-1951(89)90156-X.

Lachenbruch, A. L., and P. Morgan (1990), Continental extension, magmatism and elevation: Formal relations and rules of thumb, *Tectonophysics*, *174*, 39–62, doi:10.1016/0040-1951(90)90383-J.

La Femina, P. C., T. H. Dixon, and W. Strauch (2002), Bookshelf faulting in Nicaragua, *Geology*, *30*(8), 751–754.

MacKenzie, L. S., G. A. Abers, S. Rondenay, K. M. Fischer, E. M. Syracuse, J. M. Protti, V. Gonzalez, and W. Strauch (2007), Crustal thickness along the Central American volcanic front, *Eos Trans. AGU*, *88*(52), Fall Meet. Suppl., Abstract T43C-07.

Mann, P., R. Rogers, and L. Gahagan (2007), Overview of plate tectonic history and its unresolved tectonic problems, in *Central America: Geology, Resources and Hazards*, edited by J. Bundshuh and G. Alvarado, pp. 201–237, Taylor and Francis, New York.

Martin, H. (1986), Effect of steeper archean geothermal gradient on geochemistry of subduction-zone magmas, *Geology*, *14*, 753–756, doi:10.1130/0091-7613(1986)14<753:EOSAGG>2.0.CO;2.

Matumoto, T., M. Othake, G. Latham, and J. Umana (1977), Crustal structure of southern Central America, *Bull. Seismol. Soc. Am.*, *67*, 121–134.

McBirney, A., and H. Wiliams (1965), Volcanic history of Nicaragua, *Univ. Calif. Publ. Geol. Sci.*, *55*, 1–65.

McKenzie, D. (1978), Some remarks on the development of sedimentary basins, *Earth Planet. Sci. Lett.*, *40*, 25–32, doi:10.1016/0012-821X(78)90071-7.

McLennan, S., and S. Taylor (1982), Geochemical constrains on the growth of continental crust, *Rev. Geophys.*, *90*, 347–361.

Meschede, M., and W. Frisch (1998), A plate-tectonic model for the Mesozoic and Early Cenozoic history of the Caribbean plate, *Tectonophysics*, *296*, 269–291, doi:10.1016/S0040-1951(98)00157-7.

Pindell, J., and J. F. Dewey (1982), Permo-Triassic reconstruction of western Pangea and the evolution of the Gulf of Mexico/Caribbean region, *Tectonics*, *1*, 179–212, doi:10.1029/TC001i002p00179.

Plank, T., and C. H. Langmuir (1998), The chemical composition of subducting sediment and its consequences for the crust and mantle, *Chem. Geol.*, *145*, 325–394, doi:10.1016/S0009-2541(97)00150-2.

Plank, T., V. Balzer, and M. Carr (2002), Nicaraguan volcanoes record paleoceanographic changes accompanying closure of the Panama gateway, *Geology*, *30*, 1087–1090, doi:10.1130/0091-7613(2002)030<1087:NVRPCA>2.0.CO;2.

Protti, M., F. Gundel, and K. McNally (1994), The geometry of the Wadati-Benioff zone under southern Central America and its tectonic significance-Results from a high-resolution local seismographic network, *Phys. Earth Planet. Inter.*, *84*, 271–287, doi:10.1016/0031-9201(94)90046-9.

Protti, M., S. Y. Schwartz, and G. Zandt (1996), Simultaneous inversion for earthquake location and velocity structure beneath central Costa Rica, *Bull. Seismol. Soc. Am.*, *86*, 19–31.

Quintero, R., and O. Kulhanek (1998), Pn-wave observations in Costa Rica, *Geofis. Int.*, *37*, 171–182.

Ranero, C. R., R. von Huene, E. Flueh, M. Duarte, D. Baca, and K. McIntosh (2000), A cross section of the convergent Pacific margin of Nicaragua, *Tectonics*, *19*, 335–357, doi:10.1029/1999TC900045.

Reymer, A., and G. Schubert (1984), Phanerozoic addition rates to the continental crust and crustal growth, *Tectonics*, *3*, 63–77, doi:10.1029/TC003i001p00063.

Rondenay, S., M. G. Bostock, and K. M. Fischer (2005), Multichannel inversion of scattered teleseismic body waves: Practical considerations and applicability, in *Seismic Earth: Array Analysis of Broadband Seismograms*, *Geophys. Monogr. Ser.*, vol. 157, edited by A. Levander and G. Nolet, pp. 187–203, AGU, Washington, D. C.

Rossi, G., G. A. Abers, S. Rondenay, and D. H. Christensen (2006), Unusual mantle Poisson's ratio, subduction, and crustal structure in central Alaska, *J. Geophys. Res.*, *111*, B09311, doi:10.1029/2005JB003956.

Rudnick, R. L. (1995), Making continental crust, *Nature*, *378*, 571–578, doi:10.1038/378571a0.

Rychert, C., K. M. Fischer, G. A. Abers, T. Plank, E. M. Syracuse, M. Protti, V Gonzalez, and W. Strauch (2008), Strong along-arc variations in attenuation in the mantle wedge beneath Costa Rica and Nicaragua, *Geochem. Geophys. Geosyst.*, doi:10.1029/2008GC002040, in press.

Saginor, I. (2007), Episodic volcanism and geochemistry in western Nicaragua, *Eos Trans. AGU*, *88*(52), Fall Meet. Suppl., Abstract T41C-0708.

Sallares, V., J. J. Danobeitia, E. R. Flueh, and G. Leandro (1999), Seismic velocity structure across the middle American landbridge in northern Costa Rica, *J. Geodyn.*, *27*, 327–344, doi:10.1016/S0264-3707 (98)00007-6.

Sheehan, A. F., G. A. Abers, C. H. Jones, and A. L. Lerner-Lam (1995), Crustal thickness variations across the Colorado Rocky Mountains from teleseismic receiver functions, *J. Geophys. Res.*, *100*(B10), 20,391–20,404.

Sinton, C. W., R. A. Duncan, and P. Denyer (1997), Nicoya Peninsula, Costa Rica: A single suite of Caribbean oceanic plateau magmas, *J. Geophys. Res.*, *102*, 15,507–15,520.

Suyehiro, K., N. Takahashi, Y. Ariie, Y. Yokoi, R. Hino, M. Shinohara, T. Kanazawa, N. Hirata, H. Tokuyama, and A. Taira (1996), Continental crust, crustal underplating, and low-Q upper mantle beneath an oceanic island arc, *Science*, *272*, 390–392, doi:10.1126/science.272.5260.390.

Syracuse, E. M., and G. A. Abers (2006), Global compilation of variations in slab depth beneath arc volcanoes and implications, *Geochem. Geophys. Geosyst.*, *7*, Q05017, doi:10.1029/2005GC001045.

Syracuse, E. M., G. A. Abers, K. Fischer, L. MacKenzie, C. Rychert, M. Protti, V. González, and W. Strauch (2008), Seismic tomography and earthquake locations in the Nicaraguan and Costa Rican upper mantle, *Geochem. Geophys. Geosyst.*, *9*, Q07S08, doi:10.1029/2008GC001963.

Taira, A., et al. (1998), Nature and growth rate of the northern Izu-Bonin (Ogasawara) arc crust and their implications for continental crust formation, *Isl. Arc*, *7*, 395–407, doi:10.1111/j.1440-1738.1998.00198.x.

Takei, Y. (2002), Effect of pore geometry on VP/VS: From equilibrium geometry to crack, *J. Geophys. Res.*, *107*(B2), 2043, doi:10.1029/2001JB000522.

Taylor, S. (1977), Island arc models and the composition of continental crust, in *Island Arcs, Deep Sea Trenches and Back-Arc Basins*, *Maurice Ewing Ser.*, vol. 1, edited by M. Talwani and W. C. Pitman, pp. 325–335, AGU, Washington, D. C.

Taylor, S., and S. McLennan (1981), The composition and evolution of continental crust; Rare earth element evidence from sedimentary rocks, *Philos. Trans. R. Soc. London*, *301*, 381–399, doi:10.1098/rsta.1981.0119.

Turner, H. L.III, P. LaFemina, A. Saballos, G. S. Mattioli, P. E. Jansma, and T. Dixon (2007), Kinematics of the Nicaraguan forearc from GPS geodesy, *Geophys. Res. Lett.*, *34*, L02302, doi:10.1029/2006GL027586.

vanDecar, J. C., and R. S. Crosson (1990), Determination of teleseismic relative phase arrival times using multi-channel

cross-correlation and least-squares, *Bull. Seismol. Soc. Am.*, *80*, 150–169.

van Wyk de Vries, B. (1993), Tectonics and magma evolution of Nicaraguan volcanic systems, Ph.D. thesis, Open Univ., Milton Keynes, UK.

von Huene, R., and D. W. Scholl (1991), observations at convergent margins concerning sediment subduction, subduction erosion, and the growth of continental crust, *Rev. Geophys.*, *29*, 279–316, doi:10.1029/91RG00969.

Walther, C. H. E., E. R. Flueh, C. R. Ranero, R. von Huene, and W. Strauch (2000), Crustal structure across the Pacific margin of Nicaragua: Evidence for ophiolitic basement and a shallow mantle sliver, *Geophys. J. Int.*, *141*, 759–777, doi:10.1046/j.1365-246x.2000.00134.x.

Weinberg, R. F. (1992), Neotectonic development of western Nicaragua, *Tectonics*, *11*, 1010–1017, doi:10.1029/92TC00859.

Zhu, L. P., and H. Kanamori (2000), Moho depth variation in southern California from teleseismic receiver functions, *J. Geophys. Res.*, *105*, 2969–2980.